Rivista Italiana di Paleontologia e Stratigrafia	volume 115	no. 1	2 pls.	pp. 67-85	March 2009

LATE EOCENE TO OLIGOCENE PRESERVATION HISTORY AND BIOCHRONOLOGY OF CALCAREOUS NANNOFOSSILS FROM PALEO-EQUATORIAL PACIFIC OCEAN SEDIMENTS

TEODORA BLAJ [1]*, JAN BACKMAN [1] & ISABELLA RAFFI [2]

Received: June 23, 2008; accepted: November 17, 2008

Key words: Calcareous nannofossils, preservation, biochronology, ODP Site 1218, paleo-equatorial Pacific Ocean, late Eocene, Oligocene, astronomical time scale.

Abstract. A continuous late Eocene through Oligocene carbonate sequence was recovered at Ocean Drilling Program (ODP) Site 1218 in the paleo-equatorial Pacific Ocean. The preservation history of selected calcareous nannofossil species across the Eocene/Oligocene (E/O) boundary is presented together with late Eocene and Oligocene calcareous nannofossil biochronology. The astronomically calibrated timescale of Pälike et al. (2006) is used here. Across the E/O boundary, placolith preservation is controlled by variation in carbonate content. Taxa less prone to dissolution are *Reticulofenestra umbilicus*, *Coccolithus pelagicus, Ericsonia formosa* and *Dictyococites bisectus*, while *Cyclicargolithus floridanus* is more susceptible to dissolution. A biochronologic framework has been established for the following taxa: the highest occurrences (HO) of *Discoaster barbadiensis* (34.773 Ma), *D. saipanensis* (34.435 Ma), *E. formosa* (32.919 Ma), *R. umbilicus* (32.021 Ma), *Sphenolithus predistentus* (26.928 Ma), *S. distentus* (26.812 Ma), and *S. ciperoensis* (24.432 Ma), and the lowest occurrences (LO) of *S. distentus* (29.997 Ma) and *S. ciperoensis* (27.142 Ma). The first consistent appearance of *Triquetrorhabdulus carinatus* occurs at 26.556 Ma, while the onset of the peak interval of *T. carinatus* was determined at 24.669 Ma. Biochronological comparisons are made with other sites from the Atlantic Ocean. A *Triquetrorhabdulus* morphotype, labeled as *T.* aff. *carinatus*, was recorded for the first time in the studied sediments, and precedes the LO of *T. carinatus* by ~ 0.7 Myr. Its stratigraphic range has a duration of about 3.3 Myr. *T.* aff. *carinatus* disappears concomitantly with the beginning of a sharp increase in abundance of *T. carinatus*.

Riassunto. Nel presente lavoro vengono riportati i risultati di uno studio sulle associazioni a nannofossili calcarei osservate nell'intervallo di transizione Eocene/Oligocene in una successione sedimentaria profonda, recuperata nel Site 1218 dell'Ocean Drilling Program (ODP) nell'Oceano Pacifico equatoriale. Sono state svolte analisi di dettaglio sullo stato di conservazione delle associazioni, strettamente legato al contenuto in carbonato registrato nell'intervallo corrispondente al limite Eocene/Oligocene. Lo studio biostratigrafico dei nannofossili calcarei ha permesso l'acquisizione di nuovi dati biocronologici riguardanti i seguenti bio-orizzonti: HO (Highest Occurrence - scomparsa) *Discoaster barbadiensis* (34.773 Ma), HO *D. saipanensis* (34.435 Ma), HO *Ericsonia formosa* (32.919 Ma), HO *Reticulofenestra umbilicus* (32.021 Ma), LO (Lowest occurrence - comparsa) *Sphenolithus distentus* (29.997 Ma), LO *Sphenolithus ciperoensis* (27.142 Ma), HO (scomparsa) *Sphenolithus predistentus* (26.928 Ma), HO (scomparsa) *S. distentus* (26.812 Ma), HO *S. ciperoensis* (24.432 Ma). Questi dati sono stati confrontati con la biocronologia a nannofossili ottenuta in altre successioni oceniche profonde delle medie e basse latitudini. La prima comparsa di *Triquetrorhabdulus carinatus* è stata registrata a 26.556 Ma, e l'analisi quantitativa svolta ha permesso di determinare con precisione l'inizio dell'intervallo di massima abbondanza (Acme) di questo taxon, datata a 24.669 Ma. Un morfotipo di *Triquetrorhabdulus*, denominato *Triquetrorhabdulus* aff. *carinatus* e riconosciuto per la prima volta nei sedimenti in esame, precede la comparsa di *T. carinatus* di ~ 0.7 Myr. Questo morfotipo, che presenta un intervallo di distribuzione stratigrafica di 3.3 Myr, mostra un netto declino, seguito dalla successiva scomparsa, in corrispondenza dell'Acme di *T. carinatus*, del quale potrebbe rappresentare il progenitore.

Introduction

ODP Site 1218 recovered a complete Eocene through Oligocene sediment sequence from the near-equatorial Pacific Ocean (Lyle et al. 2002; Wilson et al. 2006; Pälike et al. 2006). Site 1218 was drilled at 8°53.378′ N; 135°22.00′ W (Fig. 1) in a water depth of 4826 m. The late Eocene through Oligocene time interval studied here, from ca. 35 Ma to 23 Ma (Fig. 2), is

1 * Corresponding author. Department of Geology and Geochemistry, Stockholm University, SE-106 91 Stockholm, Sweden.
E-mail address: teodora@geo.su.se
2 Dipartimento di Geotecnologie per l'Ambiente e il Territorio, Università "G. d'Annunzio" di Chieti-Pescara, Via dei Vestini 31, 66013 Chieti, Italy

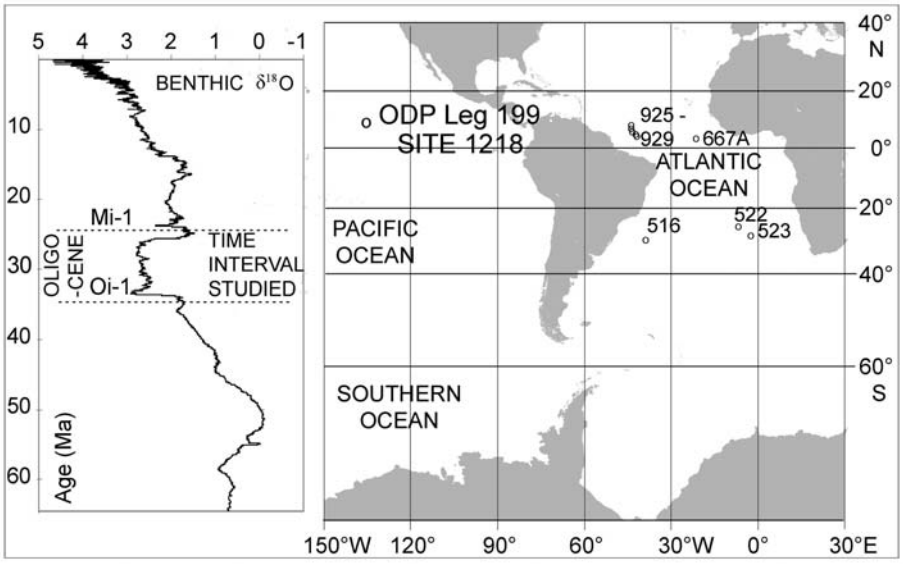

Fig. 1 - The location of ODP Site 1218, and Atlantic ODP and DSDP drill sites discussed in this paper. The map is modified from http://www.iodp-usio.org/. Insert figure shows the time interval studied here together with the global benthic stable isotope record for the Cenozoic compiled by Zachos et al. (2001); Oi-1=Oligocene Isotope event-1; Mi-1=Miocene Isotope event-1.

characterized by changes in the ocean carbonate system, and hence the global carbon cycle, the build-up and subsequent variability of continental ice volumes, global sea-level as well as major re-organizations of plankton communities and surface water conditions (e.g. Miller et al. 1991; Zachos et al. 2001; Wade & Pälike 2004; Coxall et al. 2005).

The Oligocene is an interval of low calcareous nannofossils species diversity, and the number of biostratigraphic markers used for this interval is low compared to other Cenozoic epochs (Perch-Nielsen 1985). The biochronology of Oligocene marker species has been documented in previous studies from different latitudes (e.g., Martini 1971; Bukry 1975; Backman 1987; Wei & Wise 1989; Olafsson & Villa 1992; Berggren et al. 1995; Shackleton et al. 1999). The Oligocene sequence recovered from Site 1218 shows sedimentation rates of about 15 m Myr^{-1}. This sequence is characterized by an unambiguous magnetostratigraphic record with distinct reversal boundaries (Lanci et al. 2005), clear orbital cycles which have permitted orbital tuning (Wade & Pälike 2004; Pälike et al. 2006), and abundant calcareous nannofossils (Lyle et al. 2002; Wilson et al. 2006). The aims of this study are: (i) to carry out morphometric measurements of the genus *Reticulofenestra* in order to determine the size variability in the *R. umbilicus-R. hillae* plexus, (ii) to analyze in detail the variability in preservation of calcareous nannofossils across the E/O boundary interval and (iii) to establish a detailed biochronology of latest Eocene and Oligocene calcareous nannofossils.

Material and Methods

A total of 1484 samples was analyzed from 101.15 to 247.54 revised meter composite depth (rmcd) in the composite sediment section of Site 1218, spliced together from Holes 1218A, 1218B and 1218C (Pälike et al. 2006).

Samples data are stored on the site http://www.pangaea.de/ and on the RIPS repository data (http://users.unimi.it/rips/115/115N1.htm).

The studied section corresponds to the time interval from 35.025 Ma to 23.406 Ma. An average sample spacing of 10 cm was used, which corresponds to an average duration of about 7.8 kyrs. Smear-slides were prepared from all samples using standard methods (e.g., Haq & Lohmann 1976; Perch-Nielsen 1985; Bown 1998). All smear-slides were analyzed using a Leica DMLP polarizing light microscope at x1000 magnification.

For the biochronologic study, semi-quantitative data on the index species were obtained using the methodology of Backman & Shackleton (1983), with abundances expressed as number of specimens per mm^2. The reproducibility and accuracy of this method was recently addressed by Blaj & Henderiks (2007). All index species were counted using between 50 and 10 fields of view (FOV) which had a relatively constant nannofossil density, averaging about 50 specimens/FOV. Most samples were investigated using 25 FOV. Ten FOV were counted when the species became dominant (>50 specimens/FOV), whereas 50 FOV were counted across the lowest and highest occurrences of index species. The data was then expressed relative to the unit area of slide examined (number of specimens per mm^2).

The terms LO and HO are used here to indicate biohorizones which define the lowest and highest occurrence of the marker species, respectively. Abundances of each species were converted to number of specimens per mm^2 and plotted against the estimated age using the Pälike et al. (2006) age model for ODP Site 1218.

A morphometric study of the genus *Reticulofenestra* was carried out on 10 samples (Appendix A) from different stratigraphic horizons. Over 100 specimens of the *R. umbilicus-R. hillae* plexus, plus 100 specimens of the smaller *Reticulofenestra* spp. group were randomly chosen and photographed in each sample using a Leica DFC 320 digital camera. Measurements of total placolith length and width, and total length and width of the central opening, on calibrated digital images were performed using the program ImageJ freeware. The calibrated pixel resolution was 0.054 μm.

Additional seventy-six (76) samples (Appendix A) were selected for analyzing the dissolution and re-appearance patterns of the calcareous nanofossils and planktonic foraminifera over an interval of 1 Myr (34.63 Ma to 33.63 Ma) across the E/O boundary. This interval shows the largest changes in carbonate contents, from virtually 0% to values as high as 90% (Fig. 2). The variability in preservation has been

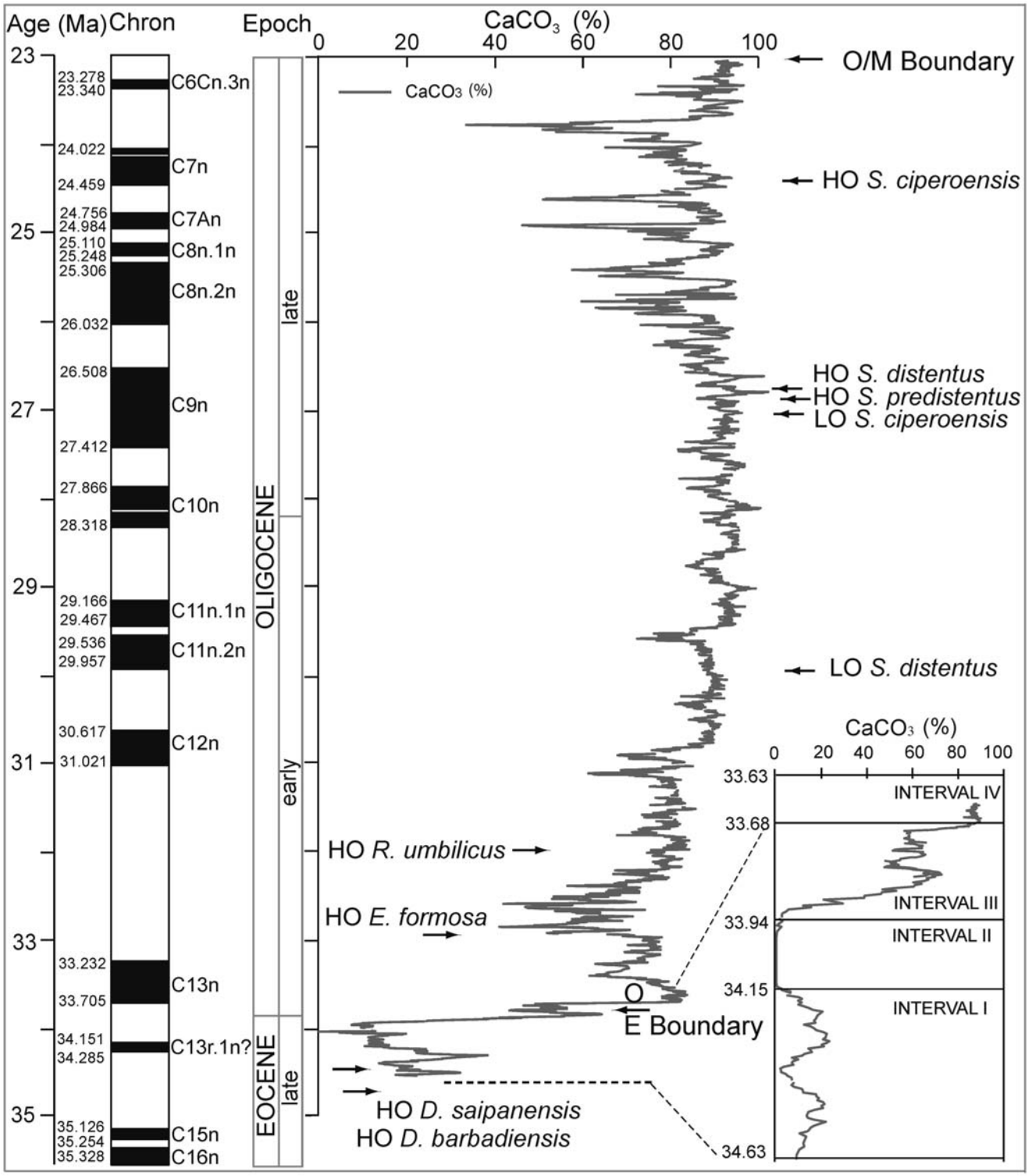

Fig. 2 - Magnetostratigraphy, calcium carbonate content and positions of biohorizons determined from Site 1218. Intervals I-IV across the E/O boundary is inserted (Chapter 3.2); the curve represents carbonate values (%). O/M boundary = Oligocene/Miocene boundary.

expressed in terms of the proportion (%) between complete and broken placolith of the following taxa: the *R. umbilicus-R. hillae* plexus, *Ericsonia formosa*, *Coccolithus pelagicus*, the *Dictyococcites* group *(D. bisectus, D. hesslandii* and *D. scrippsae), Cyclicargolithus floridanus. Sphenolithus predistensus, S. moriformis, D. saipanensis*, and *Discoaster* spp. were analyzed as proportion between presence/absence of taxa and their relative abundances. The counts were made in 25 FOV, with relatively constant nannofossil density in carbonate-bearing samples. The frequency distribution of complete versus broken specimens was expressed as cumulative percentage and plotted against age. For determining when the first planktonic foraminifera re-appeared in the record, eight samples were sieved over a 63 μm sieve using calcite buffered water.

The calcium carbonate values ($CaCO_3$ weight %) from Site 1218 were taken from the Pangaea database (www.pangaea.de).

Taxonomic notes

The taxonomy follows Perch-Nielsen (1985) and Aubry (1984, 1988, 1989, 1990, 1999). Studied taxa are listed in Appendix A. Sphe-

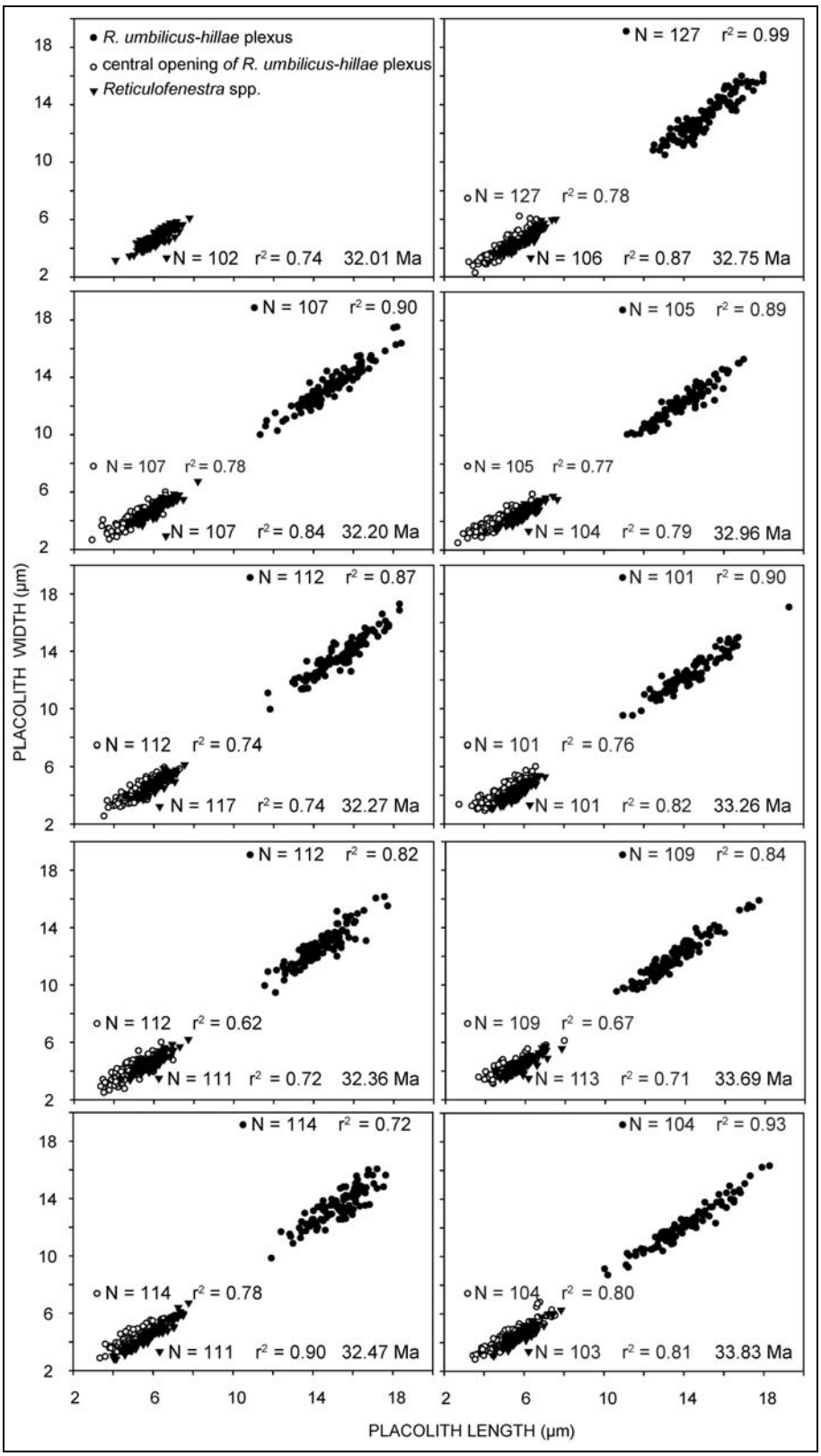

Fig. 3 - Morphometric measurements of the *R. umbilicus-R. hillae* plexus and *Reticulofenestra* spp. in ten different samples.

noliths are important for the subdivision of the Oligocene Series (Bramlette & Wilcoxon 1967; Martini 1971; Bukry 1975; Okada & Bukry 1980). The morphological features described in Perch-Nielsen (1985) and Roth et al. (1971) were used here to distinguish between *S. predistentus*, *Sphenolithus distentus* and *Sphenolithus ciperoensis. Sphenolithus predistentus* is characterized by a low proximal column and a conical apical spine with a broad base and the extinction lines between the proximal column and the apical spine is nearly straight, when viewed at 45° to the polarizers. *Sphenolithus distentus* has a generally large apical spine and the extinction lines between the proximal column and the apical spine are V-shaped. *Sphenolithus ciperoensis* is characterized by a small apical spine and nearly X-shaped extinction lines. Transitional forms between *S. predistentus* and *S. distentus* were observed. The distinction between the two forms was made based on the features described by Roth et al. (1971, pp. 1106, fig. 5). If the angle between the extinction line at the base of the apical spine is 90° or less with the

median axis of the sphenolith the forms are assigned to *S. predistensus.* If the extinction angle is more then 90° and forming a clear V-shape the forms are assigned to *S. distentus*. However, numerous forms having only a slight angle, just a little over 90°, these forms were referred to as transitional forms between *S. predistensus* and *S. distentus*. Six sphenolith events were identified at Site 1218: (1) the LO of transitional forms between *S. predistentus* and *S. distentus*, (2) the lowest continuous occurrence (LCO) of *S. distensus*, (3) the LO of *S. ciperoensis*, (4) the HO of *S. predistensus*, (5) the HO of *S. distensus* and (6), the HO of *S. ciperoensis.*

Biochronological comparisons with earlier timescales

The astronomically calibrated timescale of Pälike et al. (2006) is used. Comparisons are made with estimates derived from two previous timescales, namely Berggren et al. (1985) and Berggren et al. (1995). The three different timescale are referred to in the text by the first initial of the author name and the year of publication, as following: Pälike et al. (2006) = P06, Berggren et al. (1985) = B85 and Berggren et al. (1995) = B95.

Age estimates in B85 and B95 were based on the use of linear interpolation between nearest geomagnetic reversal boundaries. Therefore, the precision of the age estimates in the B85 and B95 timescales depends on the sample spacing used in the pertinent studies and the error introduced when assuming constant sedimentation rates between the reversal boundaries. Age estimates using the B85 or B95 timescales are therefore generally an order of magnitude less precise compared to the estimates determined using the P06 timescale, which is astronomically tuned. An age estimate generated using B85 is first converted to B95 using linear interpolation, which is further converted to P06 following data available in the Pangaea database (www.pangaea.de). All B85 and B95 age estimates are converted to the P06 timescale.

Results

Morphometric measurements of *Reticulofenestra* spp.

Reticulofenestra umbilicus is distinguished from other related taxa by its larger size. Proportional changes in placolith size and central opening size within this genus are used for taxonomic purposes. Backman & Hermelin (1986) suggested the use of a lower placolith length of 14 µm for the identification of the first appearance of *R. umbilicus. Reticulofenestra hillae* is a variety of *R. umbilicus* having a thicker collar around the central opening and thus a smaller central opening (Bukry & Percival 1971; Backman & Hermelin 1986).

Morphometric measurements of *Reticulofenestra* spp., and the *R. umbilicus* group (Pl. 1, fig. 1-3) were made on 10 samples taken from different stratigraphic levels. Placolith length shows a high correlation with placolith width (r^2=0.87; N=9). Similarly, central opening length shows a high correlation with central opening width. Furthermore, placolith size and central opening size show similar positive slopes (Fig. 3). Placolith lengths show consistent patterns, ranging between approximately 11 µm and 18 µm for one cluster and between 4 µm and 8 µm for another cluster; the large cluster representing the *R. umbilicus* group. The small cluster may contain several described species. These are, however, difficult to distinguish using the simple morphometric characteristics adopted here. We therefore refer to this group as *Reticulofenestra* spp. This smaller morphotype has a mean value of placolith length of 5.9 µm, while the large morphotype has a mean value of placolith length of 14.5 µm.

The results of the morphometric analyses (Fig. 3) do not show any bimodal distribution among the large cluster, either in total length or central opening length. *Reticulofenestra umbilicus* and *R. hillae* could not be distinguished as two different subpopulations using these measurements. The two varieties thus appear to represent intra-specific variation rather than inter-specific variation. Consequently, we combine these two morphotypes into a single taxonomic entity, the *R. umbilicus* group. Moreover, the 14 µm size limit for the *R. umbilicus* concept is not applicable in these late Eocene and early Oligocene at Site 1218.

The return of calcareous nannofossils and planktonic foraminifers after the late Eocene shallow CCD event

The late Eocene shallow CCD becomes even shallower during the latest Eocene, marked by an interval that is barren of carbonate. The CCD begins to deepen about 130 kyrs prior to the Eocene/Oligocene (E/O) boundary. About 130 kyrs after the E/O boundary (33.79 Ma), the CCD has deepened sufficiently to permit sediment carbonate concentrations of nearly 90 % at Site 1218. This change of the CCD resulted in major improvements in the preservation of calcareous nannofossils.

Biogenic carbonate is lacking, varying between 0.2 and 2.9%, in a one meter thick interval representing about 210 kyrs, between 34.15 Ma and 33.94 Ma (Fig. 4A). Calcareous nannofossils return to the latest Eocene sediments, simultaneously with the initial sharp and rapid increase in carbonate concentration at 33.90 Ma. Planktonic foraminifers, on the other hand, return later than calcareous nannofossils. According to Lyle et al. (2002), the foraminifers returned between about 33.70 and 33.51 Ma. We had eight intervening samples, which were sieved in order to determine more precisely when the first planktonic foraminifers returned. These data places the first Oligocene planktonic foraminifers at 239.67±0.05 rmcd, that is, at 33.676±0,002 Ma. Calcareous nannofossils thus began their recovery 229 kyrs earlier (33.905 Ma) than the planktonic foraminifera, re-inforcing the insight that calcareous nannofossils are less susceptible to dissolution than planktonic foraminifers (Berger 1973).

Carbonate contents and calcareous nannofossil abundances were compared in a critical one million year long interval, from 34.63 Ma to 33.63 Ma, in which major changes occurred in both carbonate values and nannofossil abundances. Changes occur at three strati-

graphic horizons, making it possible to subdivide this one million year long period into four intervals (Fig. 4A), each with a characteristic carbonate and nannofossil abundance pattern. These four intervals are described below in a chronological order, i.e., from older to younger:

Interval I (Late Eocene: 34.63 - 34.15 Ma) Pl. 2, Fig. 10-12

Carbonate values vary from 2.3 to 22.3% in a cyclical trend. Calcareous nannofossils assemblages are characterized by strongly dissolved, fragmented and broken placoliths, and presence of a single species of discoaster in the lower part of this interval, namely *D. saipanensis,* which was overgrown by secondary calcite. Few six-rayed overgrown *Discoaster* spp. were identified in the upper part of Interval I. Placoliths are composed mainly of fragmented reticulofenestrids, *C. floridanus*, the *D. bisectus-D. hesslandii-D. scrippsae* group, *C. pelagicus* ("ghosts" - isolated proximal and/or distal shields of placoliths), and fragments of *E. formosa* (isolated proximal and/or distal shields).

Interval II (Late Eocene: 34.15 - 33.94 Ma) Pl. 2, Fig. 7-9

This interval is characterized by intense carbonate dissolution (0.2-1.7% carbonate), and therefore is virtually barren of carbonate. A few isolated unidentifiable placolith fragments were observed in this interval.

Interval III (Late Eocene and E/O boundary: 33.94 - 33.68 Ma) Pl. 2, Fig. 4-6

Carbonate values vary from 4.7 to 82.5%. The initial rise in carbonate contents is sharp, increasing to more then 50% over 66 kyrs. Nannofossil assemblages are characterized by a progressive increase of well preserved and complete placoliths, although broken/fragmented specimens are still present in high percentages. The discoasters are the first identifiable specimens to reappear, following the late Eocene barren interval.

Interval IV (Early Oligocene: 33.68 - 33.63 Ma) Pl. 2, Fig. 1-3

The base of this interval is placed where planktonic foraminifers return. This interval is characterized by high carbonate values varying from 85.5 to 89.3%. The percentage of complete calcareous nannofossil specimens dominates over broken/fragmented specimens, which show a sharp decrease.

Preservation pattern of the *R. umbilicus* group

The complete/broken pattern of this group varied in a cyclic trend with the carbonate content in Interval I (Fig. 4B), where the percentage of broken taxa represents over 55% of the assemblage. The complete specimens are dissolved and/or over-calcified and their abundance reaches over 40% of the assemblage in samples with < 20% carbonate. The recovery to complete taxa occurred over an interval of 38 kyrs, with the increase of carbonate values to 12%. The basal and middle parts of Interval III is characterized by high abundances of complete taxa, reaching from 59% up to 79% of the assemblage, where carbonate contents increase to 65%. This trend of high abundance of complete specimens is slightly decreasing towards the top of this interval, but recovers when carbonate contents increase to values over 79.2%. Complete specimens reach maximum values (90%) in Interval IV.

Preservation pattern of *Ericsonia formosa*

The number of broken *E. formosa* taxa dominates over the number of complete specimens in Interval I (Fig. 4C). The broken specimens consist mostly of isolated proximal shields. Following the barren late Eocene Interval II, the recovery of *E. formosa* from a broken appearance to complete taxa was quite sharp, occurring over a period of 66 kyrs. The base of Interval III is characterized by an increase in carbonate content and a simultaneous appearance of complete specimens of *E. formosa*. Its abundance fluctuates strongly between complete and broken specimens, with more broken specimens at the base of Interval III. The top of this interval is characterized by an increase in percentage of complete taxa. This change occurred concomitantly with increasing carbonate content, rising from values of 57% to 83% over 16 kyrs. Interval IV is characterized by having more than 90% complete specimens of *E. formosa*.

Preservation pattern of *Coccolithus pelagicus*

Coccolithus pelagicus is considered to be one of the least dissolution prone species (Berger 1973). Interval I illustrates a cyclical co-variation of complete versus brocken taxa and carbonate content (Fig. 4D). Broken specimens are dominant (90%) in this interval, in which separated distal or proximal shields are preserved. Broken specimens continue to represent a high percent of the assemblage just at the base of Interval III, in three samples with low carbonate content (12 to 46%). In the next younger sample, in which the carbonate content increases to 53%, a sharp cross-over in the assemblages is observed, with high abundance of complete specimens and a simultaneous decrease of broken specimens. The complete specimens represent 89% of the assemblage in the upper part of Interval III. Interval IV is dominated by completely preserved *C. pelagicus* (99 %).

Preservation pattern of the *Dictyococcites bisectus* group

The preservation pattern of this group varies in concert with the carbonate concentration changes in Intervals I-IV (Fig. 4E). The percentage of broken specimens represents between 50 and over 80% of the group assemblage in Interval I. A few overcalcified specimens were observed in the upper part of Interval II. A

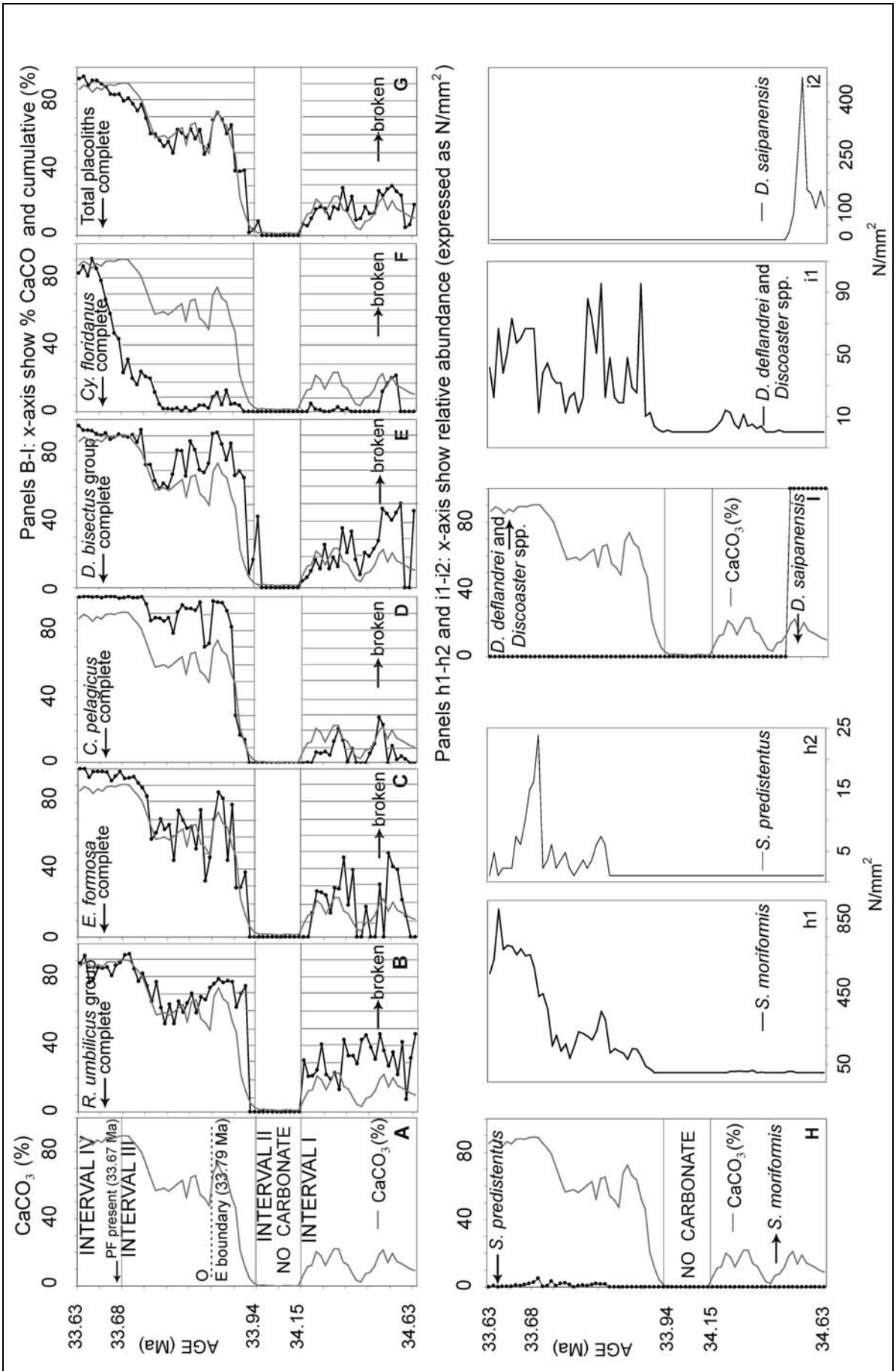

Fig. 4 - The carbonate dissolution Intervals I - IV (34.63 Ma to 33.63 Ma): (A) $CaCO_3$ (%). Cumulative frequencies (in %) of complete (area left of heavy black line with filled circles) versus broken (area with vertical lines, right of heavy black line with filled circles) specimens: (B) *R. umbilicus*, (C) *E. formosa*, (D) *C. pelagicus*, (E) *D. bisectus*, (F) *C. floridanus*, (G) Total placoliths. (H) shows abundance (as cumulative %) of *S. moriformis* versus *S. predistentus*. (I) shows abundance of *D. saipanensis* versus *D. deflandrei* and *Discoaster* spp. (0 % *D. saipanensis* implies 100 % of the *D. deflandrei* and the *Discoaster* spp. group and vice versa). Relative abundances (expressed as number of specimens/mm^2) of: (h) *S. moriformis*, (hh) *S. predistentus*, (i) *D. saipanensis*, (ii) *D. deflandrei* and the *Discoaster* spp.

sharp dominance of complete specimens occurs in Interval III. These increase proportionally with the increase in carbonate content. Interval IV is characterized by dominance of complete specimens, which represent nearly 90% of the group assemblage.

Preservation pattern of *C. floridanus*

A few complete specimens of *C. floridanus* were observed in the lower part of Interval I. Broken specimens have the central area completely dissolved. Such specimens dominate the assemblage, reaching more than 95% in the remaining part of the Interval I (Fig. 4F). A slight increase, to 10%, of complete specimens was observed in the basal part of Interval III, where carbonate content is about 70%. The recovery of *C. floridanus*, from a broken to complete specimens, occurred in the upper part of Interval III, in contrast to other placolith taxa, which began their preservation recovery in the lower part of Interval III. Although the carbonate content is high in this interval, the broken specimens dominate, with over 80% the assemblage. A sharp increase, from 20% to 50%, of complete specimens occurs in the basal part of the high carbonate content Interval IV. In the upper part of this interval, the assemblage is dominated by complete specimens.

Nannolith abundance

Cumulative frequencies of the presence/absence pattern of *S. predistentus* and *S. moriformis* and *D. deflandrei, Discoaster* spp. and *D. saipanensis* are shown in Fig. 4H and 4I. The sphenoliths assemblage is dominated by *S. moriformis*. In Interval I, the abundance of *S. moriformis* is low. However in Intervals III and IV, its relative abundance increases parallel with the increase in carbonate content (Fig. 4h). Over 300 specimens per mm^2 were observed in Interval III and more than 600 specimens in Interval IV. The first specimens of *S. predistentus* were observed in an interval of increasing carbonate content (60%), in the middle part of Interval III at about 33.78 Ma (Fig. 4hh). In this interval, the abundance of *S. predistentus* is low (5 specimens per mm^2) and the few preserved specimens are commonly overgrown. An increase in abundance is observed in Interval IV. The discoaster assemblage is represented by a single species of rosette shaped discoaster (*D. saipanensis*) and few six-rayed *Discoaster* spp. in Interval I. The abundance of *D. saipanensis* is high (100 specimens per mm^2) and reaches even higher values before its extinction (Fig 4i). Intervals III and IV are characterized by the presence of *D. deflandrei* and *Discoaster* spp. (Fig 4ii).

The Eocene/Oligocene boundary interval

The E/O boundary is defined in marine biostratigraphy by the HO of the planktonic foraminiferal genus *Hantkenina* (Coccioni et al. 1988; Premoli Silva & Jenkins 1993) at 33.790 Ma in P06. The HOs of *D. barbadiensis* and *D. saipanensis* occur shortly prior to the *Hantkenina* extinction (Perch-Nielsen 1985). At Site 1218, the stratigraphy around the E/O boundary is marked by a major change from a dark brown radiolarite to light nannofossil chalk and ooze. This change in carbonate preservation and accumulation represents a major event that has been observed in many Pacific Ocean sites (van Andel et al. 1975; Bralower et. al. 2002; Coxall et al. 2005), reflecting a major deepening of the calcite compensation depth (CCD) that occurred in two steps of 40 kyrs each separated by an intermediate plateau having a duration of about 200 kyrs (Coxall et al. 2005). The E/O boundary is inferred via cyclostratigraphy at Site 1218 (Pälike et al. 2006) because the planktonic foraminifer *Hantkenina* is not preserved at Site 1218; the boundary falls in the early part of the 200 kyrs long plateau showing intermediate carbonate contents (Coxall et al. 2005). At Site 1218, biogenic carbonate did not accumulate in a 210 kyrs long interval (34.15-33.94 Ma), characterized by a CCD level shallower than the depositional depth of Site 1218. Carbonate values varied from 2.3 to 22.5% in a cyclical way between about 34.63 and 34.15 Ma (Fig. 2, 4A). The HOs of *D. barbadiensis* and *D. saipanensis* both occur in this low carbonate interval (Fig. 5) close to each other, as noticed by Bukry (1973; 1975).

Oligocene biochronology

This study provides the first astronomically tuned age estimates of Oligocene calcareous nannofossils, continuing Neogene efforts in this direction (Raffi et al. 2006). Biochronological comparisons with other key sites from the South Atlantic are presented in Table 1.

Martini (1971) used the HO of *D. saipanensis* to define the base of Zone NP21. The HO of *D. barbadiensis* occurs at 34.773±0.018 Ma, and the extinction of *D. saipanensis* at 34.435±0.012 Ma, thus being 338 kyrs apart (Fig. 5). The latter species became extinct 645 kyrs prior to the *Hantkenina* extinction and the E/O boundary, in the relatively long, reversed Chron C13r.

The HO of *E. formosa* defines the Zones NP21/NP22 boundary of Martini (1971) and CP16b/CP16c boundary of Okada & Bukry (1980). At Site 1218, this marker species varies in abundance (Fig. 5). Its final decline and sharp extinction occurs in an interval with decreasing carbonate concentrations, from about 80 to 40% carbonate. However, the extinction of *E. formosa* does not appear to have been biased by carbonate dissolution judging from its abundance pattern and the general shape of the carbonate content curve. The extinction of *E. formosa* at Site 1218 is determined to 32.919±0.004 Ma.

The HO of *R. umbilicus* defines the Zone NP22/NP23 boundary of Martini (1971) and the CP16c/CP17

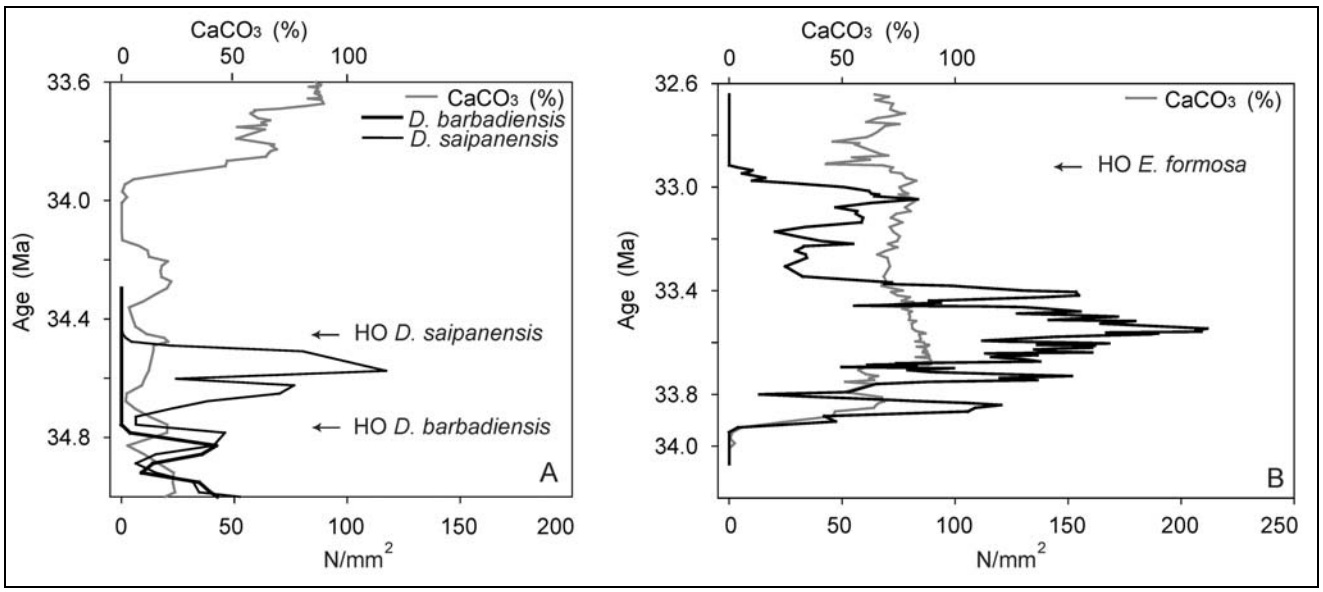

Fig. 5 - Relative abundances of *D. barbadiensis* (thick black line), *D. saipanensis* (thin black line) and *E. formosa* (right panel). Gray line represents carbonate content (%).

boundary of Okada & Bukry (1980). The range of *R. umbilicus* shows high variability in abundance (Fig. 6), with the main abundance peaks varying in what appears to be a cyclical trend. Abundances decrease gradually in the top part of the range. This species also shows discontinuous occurrences in its upper range. The extinction of *R. umbilicus* at Site 1218 is determined to 32.021±0.003 Ma.

Forms transitional between *S. predistentus* and *S. distentus* were observed well below the LO of the *S. distentus* s.s. The transitional forms show a distinct LO at 33.290±0.016 Ma. This form is common in the lower part of its range, and occurs discontinuously with lower abundances in its upper range. The last specimens were observed in a sample at 30.173±0.007 Ma (Fig. 7).

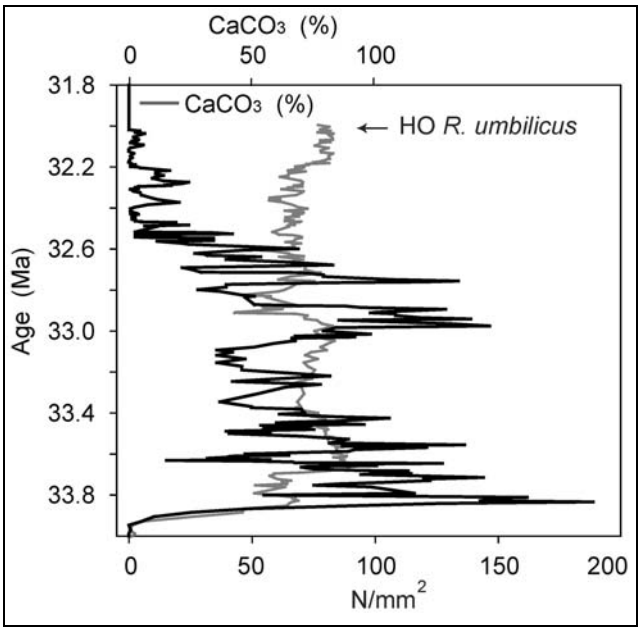

Fig. 6 - Relative abundance of *R. umbilicus*. Gray line represents carbonate contents (%).

The LO of *S. distentus* defines the Zone CP17/18 boundary in Okada & Bukry (1980). At Site 1218 the LO of *S. distentus* was placed at 29.997±0.006 Ma, which is 3293 kyrs after the appearance of the first transitional forms. *Sphenolithus distentus* shows strong abundance changes throughout its range (Fig. 7). Two main intervals of fluctuating high abundances are present (80-120 specimens/mm^2), separated by an interval of lower values (20-40 specimens/mm^2), the latter observed between 28.266 Ma and 28.097 Ma.

The LO of *S. ciperoensis* defines the top of Zones NP23 (Martini 1971) and CP18 (Okada & Bukry 1980), respectively. Discontinuous occurrences in the earliest part of its range increases the uncertainty of its true age at Site 1218. It is continuously present from 27.093±0.003 Ma (Fig. 7) in Site 1218. When the discontinuous occurrences below that horizon are taken into account, its LO can be determined to 27.142±0.052 Ma, calculated from one sample below the lowermost occurrence to the sample containing the first continuous occurrence.

Sphenolithus predistentus is not traditionally used for the subdivision of the Oligocene, but the importance of *S. predistentus* as biostratigraphic marker has been argued by, for example, Fornaciari et al. (1990) and Olafsson & Villa (1992). *Sphenolithus predistentus* shows marked fluctuations in abundance (Fig. 7), in what appears to be a cyclical fashion. In the upper part of its range, the abundance decreases sharply just prior to the extinction, estimated at 26.928±0.002 Ma. Still, judging from the data at Site 1218, the distribution of

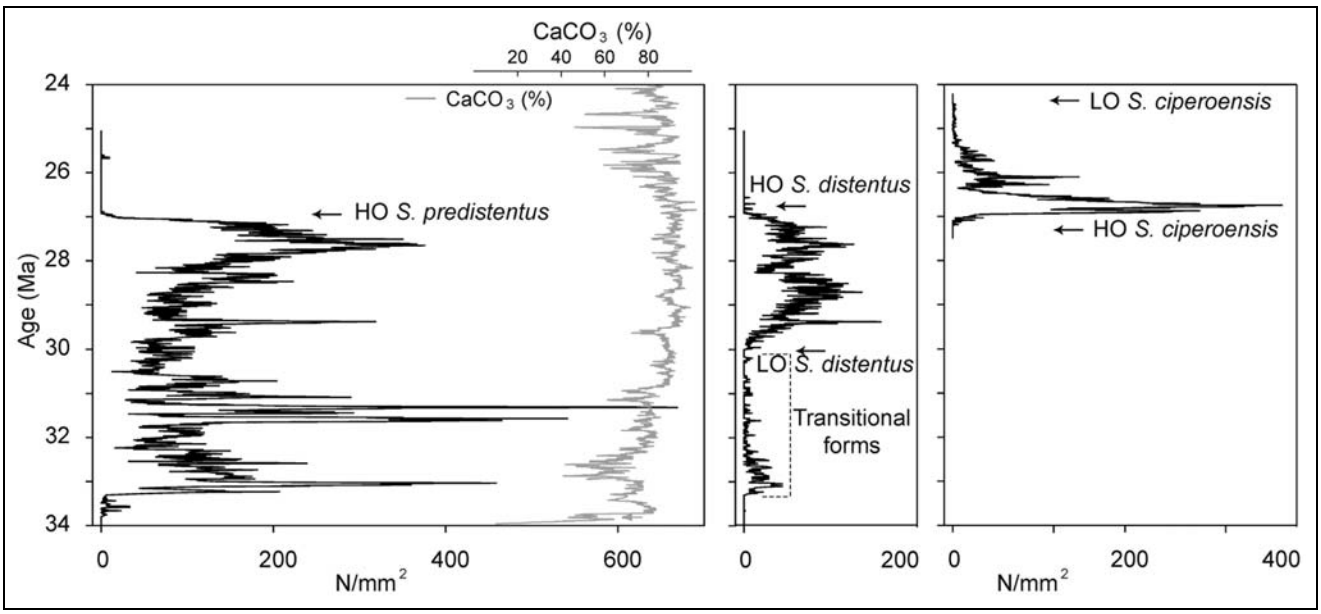

Fig. 7 - Relative abundances of *S. predistentus* (left panel), *S. distentus* and the transitional form between *S. predistentus* and *S. distentus* (middle panel), and *S. ciperoensis* (right panel). Gray line represents carbonate content (%).

S. predistentus shows a sharp final decline in abundance. Its HO therefore represents a useful biostratigraphic signal, which can be employed to approximate the Zone NP24/25 boundary and to increase the biostratigraphic resolution of the Oligocene, as previously suggested by Fornaciari et al. (1990) and Olafsson & Villa (1992).

The HO of *S. distentus* marks the NP24/NP25 and the CP19a/CP19b zonal boundaries. The end of its continuous presence is determined 26.926±0.003 Ma (Fig. 7). If the discontinuous occurrences after this sample is included, the HO of *S. distentus* is determined at 26.812±0.114 Ma, which is adopted here.

The HO of *S. ciperoensis* defines the top of Zones CP19a of Okada & Bukry (1980) and the top of NP25 of Martini (1971). The HO is determined at 24.432±0.005 Ma. This is fully compatible with the shipboard data (Pälike et al. 2006, table S2), if considering the larger depth uncertainty (1.5 m) in the shipboard determination. After 25.253 Ma, *S. ciperoensis* is present with <5 specimens mm^{-2} and shows occasionally discontinuous occurrences (Fig. 7). In fact, the abundances of *S. ciperoensis* towards the end of its range are so low that finding the absolutely last specimens in the true range of this species is difficult to reproduce precisely even if counting 50 FOV having >50 specimens/FOV. The HO of *S. ciperoensis* has an astronomically calibrated age of 24.131 Ma from Site 522 in the South Atlantic (Shackleton et al. 2000), which is 301 kyrs younger than the estimate from Site 1218. It is thus possible that the last observed specimens at Site 1218 represents a paleoecological event rather than the true extinction event of this species. This datum hence must be used with caution because of low abundances towards its uppermost range and clear diachrony between low and middle latitudes, disappearing earlier at lower latitudes.

Two *Triquetrorhabdulus* morphotypes

Triquetrorhabdulus carinatus was originally described from the western equatorial Pacific by Martini (1965) as elongated forms having "three-edged rods, with pointed, rounded or truncated ends". Martini (1965) defined the length of *T. carinatus* as being 9-15 µm, although he also mentioned that forms of up to 24 µm had been observed from Trinidad. Bramlette & Wilcoxon (1967) improved the original description by indicating that the genus *Triquetrorhabdulus* has "the optic axes of the calcite parallel to the long axis of the rod and not at right angle". Intraspecific variations of *T. carinatus* were studied by Lipps (1969). The general shape and the development of the ridges are used to distinguish between different species of *Triquetrorhabdulus* (Aubry 1988). According to Young (2008; www.nannotax.org), size differences among *T. carinatus* can be used to distinguish two main morphotypes within this species: "long thin specimens with parallel sides (entire specimens 25-50 x 1.5-2.5 microns) and shorter and broader specimens with distinct taper (15-25 x 2-4 microns)".

At Site 1218, two *Triquetrorhabdulus* morphotypes were counted separately. One was typical *T. carinatus* s.s. (Pl. 1, fig. 4-9) with distinct ridges, and ranging in length from 10 µm to 20 µm. Most specimens showed moderate to heavy calcite overgrowth. Overgrowth of secondary calcite often fills in the areas between the ridge blades; these specimens look like simple

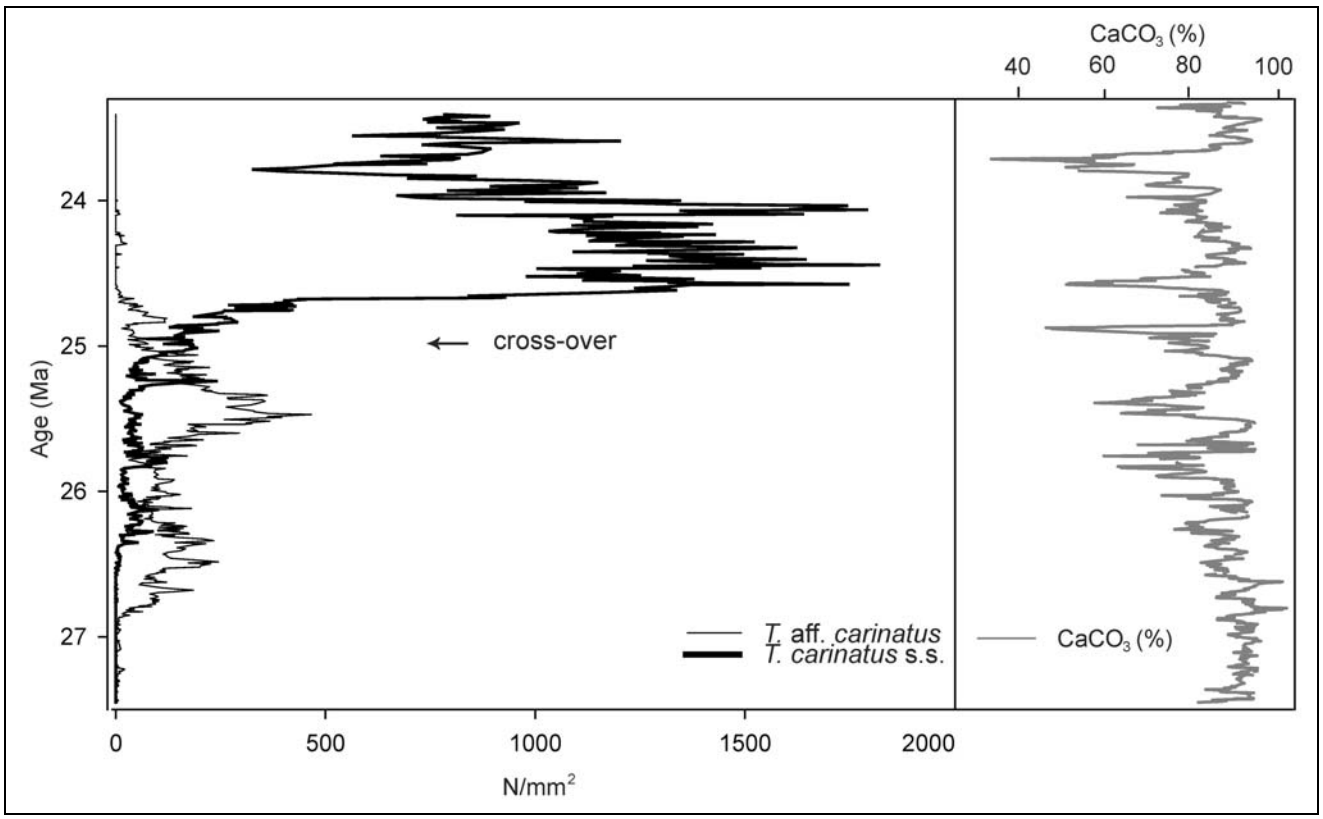

Fig. 8 - Relative abundances of *T. carinatus* s.s. and *T.* aff. *carinatus*. Right panel shows the carbonate content (%).

rods. These typical *T. carinatus* occur in low abundances in the early part of their range before becoming abundant about two million years after their first occurrence (Fig. 8). Another morphotype, which is tentatively referred to *Triquetrorhabdulus* aff. *carinatus,* (Pl. 1, fig. 10-15) was also observed. It is mainly distinguished from *T. carinatus* s.s. by its greater length (20-45 µm). The ridges are present in some specimens but are too poorly preserved to be clearly distinguished in most observed specimens. *Triquetrorhabdulus* aff. *carinatus* is typically narrower than *T. carinatus* s.s. and appears less bright in polarized light, suggesting that it is less heavily calcified. Many of the specimens of the longer morphotype appear grayer in cross-polarized light than *T. carinatus* s.s. Still, when observed in polarized light, the longer morphotype has a similar optical behavior compared with *T. carinatus* s.s, in showing maximum birefringence at 45° to the polarizers. The longer morphotype are often broken into smaller fragments, but these fragments are distinguished from typical *T. carinatus* s.s. by being narrower and less bright. Many of the presumably more complete specimens of the longer morphotype are needle-shaped, with one end thicker and hence brighter under crossed nicols, narrowing off throughout its length and becoming progressively less bright.

The two morphotypes have distinct stratigraphic ranges (Fig. 8). The first occurrence of *T.* aff. *carinatus* is characterized by a short interval of low abundance. Its first occurrence is older than 27.4 Ma. In the lower part of the range the longer morphotype co-occurs with *T. carinatus* s.s. and is consistently the more abundant of the two. A cross-over in abundance between *T.* aff. *carinatus* and *T. carinatus* s.s. occurs just before 25 Ma (Fig. 8). At the upper part of its range *T.* aff. *carinatus* shows low abundance and scattered occurrences. The last specimens of the longer morphotype were observed at 24.0 Ma, nearly five million years prior to the extinction of *T. carinatus* s.s. at 19.184 Ma (Pälike et al. 2006). The distribution of the longer morphotype, *T.* aff. *carinatus*, has not been previously employed in marine biostratigraphy.

The LO of *T. carinatus* s.s. is not used in the subdivision of the Oligocene. Its lowest occurrence in the western equatorial Pacific is slightly above the base of NP24 (Martini & Worsley 1971). At Site 1218, the LO of *T. carinatus* s.s is difficult to determine precisely, because of the presence of a nearly 0.4 Myr long initial interval of low and discontinuous abundances. Continuous occurrences began at 26.556 Ma. A step in abundance occurs at 26.372 Ma, resulting in a second interval showing abundances on the order of 10 to 450 specimens/mm^2 (24.681 Ma), which marks the beginning of a third interval representing a further sharp increase in abundance. Here, 500 to 1500 specimens/mm^2 were observed in up to 23.406 Ma (Fig. 8). We know from the

shipboard data (Lyle et al. 2002) that this high abundance interval continues to 22.159 Ma (Pälike et al. 2006). A peak value of 1818 specimens/mm^2 was observed at 24.442 Ma.

The beginning of this peak abundance interval of *T. carinatus* s.s. coincides with the final low abundance interval of *S. ciperoensis*. It appears reasonable to suggest that the latter was outcompeted by the former. Notably, the demise of *T.* aff. *carinatus* also seems to begin at the onset of the peak abundance interval of *T. carinatus* s.s. The abundance pattern of *T. carinatus* at Hole 667A in the equatorial Atlantic Ocean (Olafsson 1989) is similar to the pattern observed at Site 1218, with an initial low abundance interval followed by a peak abundance interval, although the peak interval it is not as intensive as in the equatorial Pacific.

Discussion

Placolith preservation patterns

In the interval between 34.63 and 34.15 Ma, placolith assemblages are dominated by separated and fragmented shields which belong to *E. formosa,* the *R. umbilicus* group, *C. pelagicus,* the *D. bisectus* group, and *C. floridanus*. This fragmentation of the placoliths is caused by carbonate dissolution. A return to well preserved calcareous nannofossil taxa occurs after 33.94, in parallel with increasing carbonate values. Diverse and rather well preserved assemblages are present from shortly before the E/O boundary (33.79 Ma). Preservation continues to improve with time and assemblages show a dominance of complete placoliths after 33.68 Ma, when carbonate values >80 % and when planktonic foraminifera begin to occur.

The *R. umbilicus* and *D. bisectus* groups are the first taxa showing dominance of complete placoliths shortly (3 samples; 30 cm) after the carbonate barren interval within the latest Eocene (Fig. 4B, E). The critical first better preserved sample has an estimated age of 33.90 Ma. *Ericsonia formosa* and *C. pelagicus* (Fig. 4C, D) show similar patterns five samples above the barren interval, at 33.85 Ma. These four taxa thus show distinct increases in the proportion of complete specimens shortly above the carbonate barren interval in conjunction with the rapidly increasing carbonate contents. In contrast, *C. floridanus* (Fig. 4F) is dominated by broken specimens throughout the 33.90-33.65 Ma interval, after which complete specimens become dominant. It follows that *C. floridanus* is the most dissolution prone placolith taxon in this study interval.

In summary, the cumulative percentage of all complete placoliths versus all broken placoliths closely reflects the changes in carbonate content (Fig. 4G). In fact, the two curves are so similar that the proportion between complete and broken placoliths, at least for this group of placolith taxa, appears to have potential as a proxy for carbonate contents.

Event	Magnetostratigraphically calibrated age (Ma)							Astronomically calibrated age (Ma)					
	Ref. location	B85	Conv. to P06	Diff.	B95	Conv. to P06	Diff.	S99 Atlantic (926)	Diff.	L02/P06	Diff.	This study Pacific (1218)	rmcd
HO *S. ciperoensis*	OV92 S. Atlantic (522)	25,04	23,743	0,689	24,75	24,031	0,401	24,14	0,292	24,357	0,075	**24,432**	111,19±0,05
T. carinatus peak*												**24,669**	113,85±0,05
LCO *T. carinatus*												**26,556**	138,46±0,05
HO *S. distentus*	OV92 (522)	27,71	26,016	0,796	27,5	26,924	-0,112	26,3	0,512	26,070	0,742	**26,812**	142,37±2,20
HO *S. predistentus*	OV92 (522)	28,74	26,953	-0,025	27,5	26,924	0,004					**26,928**	144,62±0,05
LO *S. ciperoensis*	OV92 (522)	29,38	27,532	-0,390	29,9	29,728	-2,586	26,9	0,242	27,048	0,094	**27,142**	147,32±0,65
LO *S. distentus*	OV92 (522)	33,91	30,622	-0,625				29,4	0,597	29,892	0,105	**29,997**	192,07±0,05
HO transitional Sp->Sd												**30,173**	194,38±0,05
LO transitional Sp->Sd												**33,290**	234,24±0,05
HO *R. umbilicus*	B87 S. Atlantic (522, 523)	33,80	31,788	0,233	31,3	31,407	0,614	32,3	-0,279	32,180	-0,159	**32,021**	218,43±0,05
	WW89 (516)	34,6	32,466	-0,445	32,3	32,352	-0,331						
HO *E. formosa*	B87 (522, 523)	34,87	32,668	0,251	32,8	32,822	0,097	33,0	-0,081	32,975	-0,056	**32,919**	231,34±0,05
	WW89 (516)	35,10	32,921	-0,002									
HO *D. saipanensis*	B87 (522, 523)	36,72	34,409	0,026	34,2	34,367	0,068	34,4	0,035	34,430	0,005	**34,435**	245,39±0,06
	WW89 (516)	36,40	34,089	0,346									
HO *D. barbadiensis*	B87 (522, 523)	36,96	34,683	0,090	34,3	34,490	0,283			34,740	0,033	**34,773**	246,69±0,05
	WW89 (516)	36,70	34,388	0,385									

Tab. 1 - Differences in age estimates of nannofossil biohorizons between this study and a few selected other studies: Ref.=Reference and corresponding location and site; OV92=Olafsson &Villa (1992); WW89=Wei &Wise (1989); B87=Backman (1987); B85=Berggren et al. (1985); B95=Berggren et al. (1995); S99=Shackleton et al. (1999); L02=Lyle et al. (2002; shipboard) data converted to P06; Conv. to P06=all ages are converted to P06 timescale. Diff.=Difference (Myr) in age estimate between the "This study" column and the corresponding age estimate in nearest left column. The sign (-) in diff. columns indicates that the age estimate is older than this study age estimate whereas (+) indicates that the age estimate is younger than the estimate of this study. LCO=lowest continuous occurrence; Sp->Sd=*S. predistentus* to *S. distentus*; *base of peak abundance, with >900 specimens/mm^2; rmcd= revised meter composite depths.

Biochronological differences between Site 1218 and other reference sites

Age estimates derived from Site 1218 are reported (Tab. 1) and compared to biochronologies from Lyle at al. (2002), Shackleton et al. (1999), Berggren et al. (1995), Olafsson & Villa (1992), Wei & Wise (1989), and Backman (1987). All age estimates are converted to the Pälike et al. (2006; tab. S2) astronomically tuned timescale from Site 1218 in order to make comparisons meaningful.

The HO of *D. saipanensis* is a synchronous event within 68 kyrs in the tropical Pacific and Atlantic oceans, and in the middle latitude South Atlantic (Tab. 1). The 346 kyrs younger estimate from Site 516 (Wei & Wise 1989) is probably due to the poor magnetostratigraphic record at this site (Berggren et al. 1995). The HO of *D. barbadiensis* occurs 338 kyrs before the HO of *D. saipanensis* at Site 1218 (Tab. 1). Age estimates for these two events from the low and middle latitude Atlantic sites presented in Tab. 1 are consistently younger, which may suggest that the Site 1218 estimate is slightly too old. A tropical Pacific estimate derived from an interval having higher carbonate contents and better calcareous nannnofossil preservation is hence desirable in order to acquire a better constrained tropical Pacific estimate.

The HO of *E. formosa* represents a virtually synchronous event in the tropical Pacific and Atlantic oceans (Tab. 1). The only marked difference is in the western middle latitude South Atlantic, whereas it is 251 kyrs younger compared to Site 1218 in the eastern middle latitude South Atlantic. This event is generally considered to be a consistent and reliable event. The 251 kyrs younger estimate is derived from DSDP Hole 523 (Backman 1987). His data from Hole 522, where the HO of *E. formosa* is represented by a distinct event at 126.30±0.1 mbsf, however, results in an age of 32.905 Ma for this event, which is only 14 kyrs younger than the estimate from Site 1218. The discrepancy between the neighboring Sites 522 and 523 is probably caused by the slightly lower sedimentation rates in Site 523 in combination with the long duration of Chron C12r (2.39 Myr on the B85 timescale). In conclusion, *E. formosa* provides a consistent and synchronous event in the low latitude Pacific and Atlantic oceans, and in the middle latitude South Atlantic.

The HO of *R. umbilicus* is a problematic marker which is difficult to pick consistently partly because of low abundances towards the end of its range. In addition, this taxon is mainly distinguished from other related taxa in terms of size differences, which probably also contributes to the fairly large spread in its estimated extinction age. Estimates vary from 614 kyrs younger to 445 kyrs older than the age derived from Site 1218. Notably, the shipboard data from Site 1218 is 159 kyrs older than the result in this study (Tab. 1). This older estimate represents the last continuous occurrence of *R. umbilicus*. Clearly, the HO of *R. umbilicus* must be used with caution.

Oligocene sphenolith events and the HO of *R. umbilicus* show the largest inconsistencies between workers and regions. The only exception is the HO of *S. predistentus*, which appears to be only 25 kyrs older in the South Atlantic (Olafsson & Villa 1992, table 4; mean age derived from different publications based on, in this case, DSDP Leg 73 sites) compared to Site 1218. This difference is considered negligible, and the HO of *S. predistentus* thus appears to represent the most consistent Oligocene sphenolith marker in the middle latitude South Atlantic and tropical Pacific Ocean.

The last continuous occurrence of *S. distentus* is observed at 26.926 Ma at Site 1218, which is followed by an interval of discontinuous and low abundances. This species has not been observed above 26.563 Ma. The mean age of this indistinct event is thus 26.812±0.114 Ma. The LO of *S. ciperoensis* shows the single largest age difference, in being 2586 kyrs older (Berggren et al. 1995) compared to the estimate derived from Site 1218. Its first continuous occurrence was observed at 27.090 Ma, and the absolutely lowest specimens at 27.194 Ma. The mean age of this event is thus placed at 27.142±0.052 Ma. This species seems to arrive to the tropical western Atlantic even later by 242 kyrs (Shackleton et al. 1999) (Tab. 1). The oldest accurate estimate for the evolutionary appearance of *S. ciperoensis* is at 27.532 Ma, derived from DSDP Hole 522 in the South Atlantic (Olafsson & Villa 1992), thus arriving 390 kyrs earlier at this site compared to Site 1218. There is a long interval of transitional forms, encompassing 3117 kyrs, between *S. predistentus* and *S. distentus*. The first distinct *S. distentus* occurs at 29.997±0.006 Ma. It follows that this event likely is picked differently by different workers (Tab. 1). This event can not be used for accurate biochronologic subdivision of Oligocene time.

The oldest estimate of the HO of *S. ciperoensis* is from this study, which is, on the average, 461 kyrs older compared to other estimates shown in Tab. 1. The small size of this species in tropical regions combined with its rare abundances towards its upper range makes it difficult to pick this event consistently. The estimate from Site 1218 thus does not represent the extinction of this species, but probably a paleoecologically caused exclusion from the tropical assemblages; it survived for about half a million years in the South Atlantic (Olafsson & Villa 1992).

Comparisons of age estimates derived from astro- and magnetochronologies

Differences in age estimates of calcareous nannofossil events based on the astrochronological tuning, on

Chron & Event	rmcd	Tuned Age (Ma)	Sed. Rate (m/Myr)*	Magn. strat. Age (Ma)	Diff.	Duration (Myr) polarity zone
Top C7n.2n	108,17	24,147	11,2			0,312
Base C7n.2n	111,67	24,459				
HO *S. ciperoensis*	111,19	24,432		24,416	0,016	
Base *T. carinatus* peak	113,85	24,669		24,653	0,016	
Top C9n	137,70	26,508	15,6			0,904
Base C9n	151,77	27,412				
HO *S. distentus*	141,59	26,812		26,758	0,054	
HO *S. predistentus*	144,62	26,928		26,953	-0,025	
LO *S. ciperoensis*	147,32	27,142		27,126	0,016	
Base C11n.2n	191,42	29,957	12,2			0,660
Top C12n	199,47	30,617				
LO *S. distentus*	192,07	29,997		30,010	-0,013	
HO trans. Sp->Sd	194,38	30,173		30,200	-0,027	
Base C12n	204,45	31,021	13,3			2,211
Top C13n	233,88	33,232				
HO *R. umbilicus*	218,43	32,021		32,071	-0,050	
HO *E. formosa*	231,34	32,919		33,041	-0,122	
Base C13n	240,29	33,705	4,7			1,421
Top C15n	246,98	35,126				
HO *D. saipanensis*	245,39	34,435		34,788	-0,353	
HO *D. barbadiensis*	246,69	34,773		35,064	-0,291	

Tab. 2 - Comparisons of age estimates established at Site 1218 using astronomically tuning and magnetostratigraphy. *Sed. Rate= sedimentation rate calculated from the rmcd (revised meter composite depth) and tuned age estimates of the reversal boundaries; Diff.= Difference (Myr) between the Tuned age and Magn. strat. (magnetostratigraphic age).

the one hand, and those obtained from interpolation between geomagnetic reversal boundaries, on the other, are compared from five different geomagnetic polarity zones (Tab. 2). All age estimates used are based on the Pälike et al. (2006) timescale. The relatively long polarity zone Chron C13r is characterized by low sedimentation rates (<5 m/Myr) while the Oligocene polarity zones are characterized by rates of about 13±2 m/Myr.

The average duration of the geomagnetic polarity zones from base C15n to top C7n.1n is 449 kyrs, using the P06 age estimates of the reversal boundaries, which represents a first-order degree of uncertainty of the age estimates using magnetostratigraphy. In astrobiochronology, the precision is determined by the cycle frequency, in this case obliquity, having a cycle length of 41 kyrs. The astrochronologically derived age estimates therefore are generally considered to be about an order of magnitude more precise compared to the magnetostratigraphic estimates.

The results from Site 1218 is, in this respect, somewhat surprising, because the age estimates of Oligocene calcareous nannofossil bioevents derived from linear interpolation between nearest reversal boundaries are, on the average, only 15 kyrs older compared to the corresponding age estimates derived from the astronomically tuned timescale. The average duration of the involved polarity zones (C7n.2n, C9n, C11r, and C12r) is 1022 kyrs. The almost negligible difference between the astro- and magnetochronological estimates at Site 1218 is explained by the rather uniform sedimentation rates during these Oligocene geomagnetic polarity zones, making the magnetostratigraphic age estimates converge with the astronomically tuned estimates. The variability observed, from 54 kyrs younger age (HO *S. distentus*) to 122 kyrs older age (HO *E. formosa*) (Tab. 2), thus likely represents minor changes in sedimentation rates within the polarity zones which are not resolved using the linear interpolation method.

The late Eocene sedimentation are characterized by low rates (4.7 m/Myr) and strongly variable carbonate contents. It is therefore not surprising that the largest age differences occur in the late Eocene interval, here represented by the HOs of *D. barbadiensis* (291 kyrs older) and *D. saipanensis* (353 kyrs older). The integrated effect of low and strongly variable sedimentation rates, and interpolation assuming linear sedimentation rates within the 1.421 ka long polarity zone C13r, may explain these relatively large differences in age estimates using the two methods.

Conclusions

- Calcareous nannofossils have been investigated at <8 kyrs sample resolution between 35.025 Ma and 23.406 Ma from the paleo-equatorial Pacific Ocean at ODP Site 1218. This section has been astronomically tuned (Pälike et al. 2006), providing an unprecedented age control across the E/O boundary and throughout most of the Oligocene.
- The investigated late Eocene and E/O boundary interval is characterized by changes in the CCD level, which is characterized in terms of four distinct intervals (I-IV), showing varying carbonate contents from 0% (II) to over 85% (IV).
- The preservation of nannofossils is assessed using percentages of complete versus broken/fragmented specimens of five placolith taxa. When this measure

is integrated for the five taxa, the resulting curve captures the general shape, as well as many of the details, of the carbonate content curve. The relative abundance of complete placoliths is thus strongly controlled by carbonate content.

- Of the five taxa involved, *C. floridanus* is clearly the least dissolution resistant form, showing a dominance of complete specimens only in Interval IV, having the highest carbonate content (>85%).
- A morphometric study of the *R. umbilicus* group was conducted in ten samples across the E/O boundary and in the early Oligocene. These measurements could not be used to distinguish between *R. umbilicus* and *R. hillae*, suggesting that the latter species represents a variety of the former.
- The length of the *R. umbilicus* placoliths varies from about 11 μm to 18 μm at Site 1218, suggesting that the commonly used 14 μm concept is not applicable.
- Biochronologic age estimates are established from the astronomically tuned age model and the results are compared with age estimates derived from linear interpolation using geomagnetic reversal boundaries. The largest differences occur where carbonate content varies strongly, implying changing sedimentation rates particularly in the long Chron C13r. Age estimates from the two methods converge in the Oligocene section, where sedimentation rates are virtually uniform.
- There appears to be no systematic difference in age estimates between Site 1218 on the one hand, and sites from the western tropical Atlantic and the middle latitude South Atlantic on the other hand. Most biohorizons can be considered to be by and large in synchrony in these three regions.
- Low and/or discontinuous occurrences, however, in the initial and/or final parts of the range of some species, notably *S. ciperoensis, S. distentus, R. umbilicus,* and *T. carinatus*, make it difficult to pick the associated biohorizons consistently.

Acknowledgements. The samples used in this study has been obtained from the Ocean Drilling Program. Data provided by Heiko Pälike is gratefully acknowledged. Jorijntje Henderiks is acknowledged for help with acquisition of the morphometric data. Careful reviews by Shirley van Heck, Maurizio Gaetani and an anonymous reviewer improved the manuscript. This project was financed by the Swedish Research Council and Stockholm University.

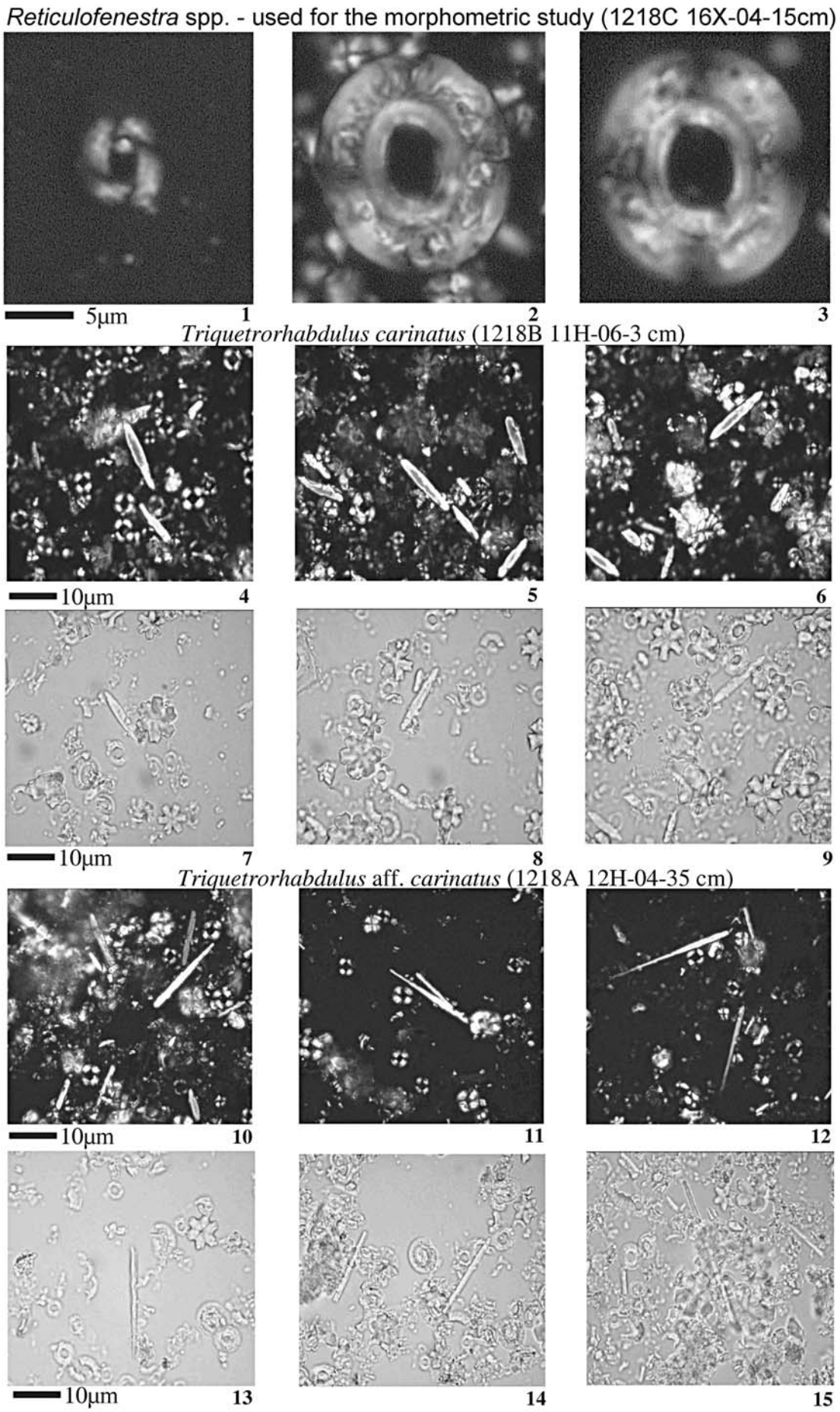
Reticulofenestra spp. - used for the morphometric study (1218C 16X-04-15cm)
5µm
1
2
3
Triquetrorhabdulus carinatus (1218B 11H-06-3 cm)
10µm
4
5
6
10µm
7
8
9
Triquetrorhabdulus aff. *carinatus* (1218A 12H-04-35 cm)
10µm
10
11
12
10µm
13
14
15

PLATE 1

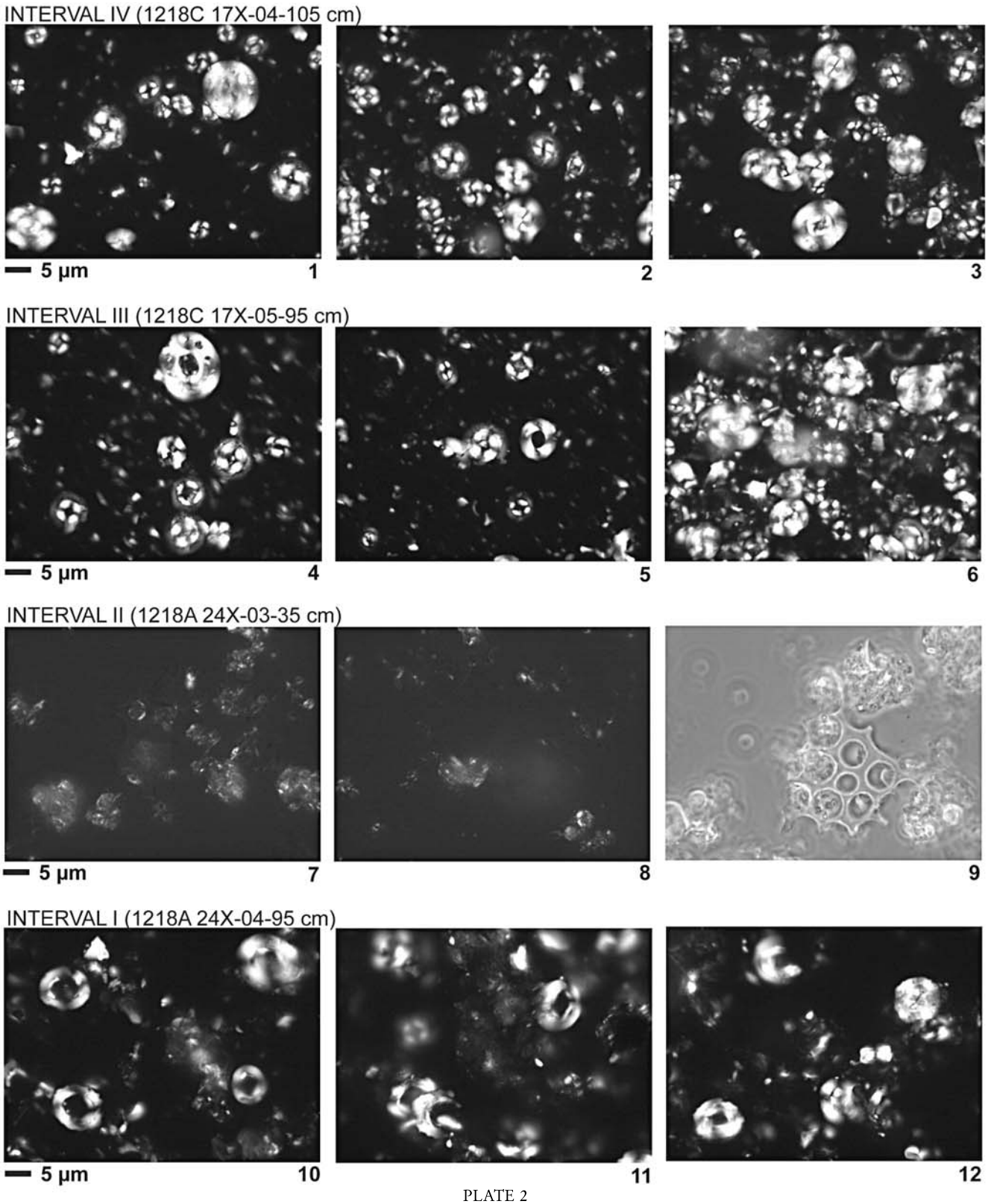
INTERVAL IV (1218C 17X-04-105 cm)
5 µm
1
2
3
INTERVAL III (1218C 17X-05-95 cm)
5 µm
4
5
6
INTERVAL II (1218A 24X-03-35 cm)
5 µm
7
8
9
INTERVAL I (1218A 24X-04-95 cm)
5 µm
10
11
12

PLATE 2

REFERENCES

van Andel T.H., Heath G.R. & Moore T.C. Jr. (1975) - Cenozoic History and Paleoceanography of the Central Equatorial Pacific Ocean: A Regional Synthesis of Deep Sea Drilling Project Data. *Mem. Geol. Soc. Am.*, 143: 1-134, Boulder.

Aubry M. P. (1984) - Handbook of Cenozoic calcareous nannoplankton, Book 1: Ortholithae (Discoasters). Micropaleontology Press, Am. Mus. Nat. Hist., New York, 265 pp.

Aubry M. P. (1988) - Handbook of Cenozoic calcareous nannoplankton, Book 2: Ortholithae (Holochoccoliths, Ceratoliths and others). Micropaleontology Press, Am. Mus. Nat. His., New York, 279 pp.

Aubry M. P. (1989) - Handbook of Cenozoic calcareous nannoplankton, Book 3: Ortholithae (Pentaliths, and others) Heliolithae (Fasciculiths, Sphenoliths and others). Micropaleontology Press, Am. Mus. Nat. His., New York, 279 pp.

Aubry M. P. (1990) - Handbook of Cenozoic calcareous nannoplankton, Book 4: Heliolithae (Helicoliths, Cribriliths, Lopadoliths and others). Micropaleontology Press, Am. Mus. Nat. His., New York, 381 pp.

Aubry M. P. (1999) - Handbook of Cenozoic calcareous nannoplankton, Book 5: Heliolithae (*Zygolithus* and *Rhabdolithus*). Micropaleontology Press, Am. Mus. Nat.l His., New York, 367 pp.

Backman J. (1987) - Quantitative calcareous nannofossil biochronology of middle Eocene through early Oligocene sediment from DSDP Sites 522 and 523. *Abh. Geol. Bundesanst.,* 39: 21-31, Wien.

Backman J. & Shackleton N.J. (1983) - Quantitative biochronology of Pliocene and early Pleistocene calcareous nannofossils from the Atlantic, Indian and Pacific oceans. *Mar. Micropaleont.,* 8: 141-170, Amsterdam.

Backman J. & Hermelin J.O.R. (1986) - Morphometry of the Eocene nannofossil *R. umbilicus* lineage and its biochronological consequences. *Palaeogeogr., Palaeoclimatol., Palaeoecol.,* 57: 103-106, Amsterdam.

Berger W.H. (1973) - Deep-sea carbonates: Pleistocene dissolution cycles. *J. Foram. Res.,* 3: 187-195, Washington.

Berggren W.A., Kent D.V. & Flynn J.J. (1985) - Jurassic to Paleogene, Part 2. Paleogene geochronology and chronostratigraphy. In: Snelling N.J. (Ed.) - The Chronology of the Geological Record. *Geol. Soc. London Mem.,* 10: 141-195, London.

Berggren W.A., Kent D.V., Swisher C.C & Aubry M. (1995) - A Revised Cenozoic Geochronology and Chronostratigraphy, pp. 129-212. In: Berggren W. A., Kent D.V., Swisher C.C, Aubry M. and Hardenbol J. (Eds) - Geochronology, Time Scales and Global Stratigraphic Correlation. *SEPM Sp. Publ.* No. 54: 129-212, Tulsa.

Blaj T. & Henderiks J. (2007) - Smear and spray preparation techniques put to the test (II): reproducibility and accuracy of calcareous nannofossil assemblage counts. *J. Nannoplankton Res.*, 29: 92-100, Washington.

Bown P.R. (1998) - Calcareous Nannofossil Biostratigraphy, British Micropalaeont. Soc. Pub. Series, Chapman and Hall (Kluwer Academic Publishers), 315 pp., London.

Bralower T.J., Premoli Silva I., Malone M.J. et al. (2002) - *Proc. ODP, Init. Repts.,* 198: College Station, TX (Ocean Drilling Program), 1-148 pp., College Station. doi:10.2973/odp.proc.ir.198.101.2002

Bramlette M.N. & Wilcoxon J.A. (1967) - Middle Tertiary calcareous nannoplankton of the Cipero section, Trinidad, W.I. *Tulane Studies in Geology and Paleontology,* 5: 93-131, New Orleans.

Bukry D. (1973) - Low-latitude coccolith biostratigraphic zonation. In: Edgar N.T., Saunders J.B., et al. - *Initial Reports of the Deep Sea Drilling Project* 15, U.S. Government Printing Office, Washington, pp. 685-703.

Bukry D. (1975) - Silicoflagellate and coccolith stratigraphy, Deep Sea Drilling Project, Leg 29. In: J.P. Kennett and R.E. Houtz et al. (Eds) - *Initial Reports of the Deep Sea Drilling Project* 29, U.S. Government Printing Office, Washington, pp. 845-872.

Bukry D. & Percival S.F. (1971) - New Tertiary calcareous nannofossils. *Tulane Studies in Geology and Paleontology,* 8: 123-146, New Orleans.

Coccioni R., Monaco P., Monechi S., Nocchi M. & Parisi G. (1988) - Biostratigraphy of the Eocene-Oligocene boundary at Massignano (Ancona, Italy). In: Premoli Silva I., Coccioni R. & Montanari A. (Eds) - The Eocene-Oligocene Boundary in the Marche-Umbria Basin (Italy). Spec. Publ., II - Int. Subcomm. Paleogr. Strat., Eocene/Oligocene Meeting, 1: 59-80.

Coxall H.K., Wilson P.A., Pälike H., Lear C.H., & Backman J. (2005) - Rapid stepwise onset of Antarctic glaciation and deeper calcite compensation in the Pacific Ocean. *Nature*, 433: 53-57, London.

Fornaciari E., Raffi I., Rio D., Villa G., Backman J. & Olafsson G. (1990) - Quantitative distribution patterns of Oligocene and Miocene calcareous nannofossils from the western equatorial Indian Ocean. *Proc. ODP, Sci. Results,* 115: College Station, TX (Ocean Drilling Program), pp. 237-254, College Station.

Haq B.U. & Lohmann G.P. (1976) - Early Cenozoic calcareous nannoplankton biogeography of the Atlantic Ocean. *Mar. Micropaleont.*, 1: 119-194, Amsterdam.

Lanci L., Parés J.M., Channell J.E.T. & Kent D.V. (2005) - Oligocene magnetostratigraphy from equatorial Pacific sediments (ODP Sites 1218 and 1219, Leg 199). *Earth Planet. Sci. Lett.*, 237: 617-634, Amsterdam.

Lipps J. H. (1969) - *Triquetrorhabdulus* and similar calcareous nannoplankton. *J. Paleont.*, 43(4): 1029-1032, Lawrence.

Lyle M., Wilson P.A., Janecek, T.R. et al. (2002) - *Proc. ODP, Init. Repts.*, 199: College Station, TX (Ocean Drilling Program), College Station. doi:10.2973/odp.proc.ir.199.2002

Martini E. (1965) - Mid-Tertiary calcareous nannoplankton from Pacific deep-sea cores. *Colston Papers*, 17: 393-411, Bristol.

Martini E. (1971) - Standard Tertiary and Quaternary calcareous nannoplankton zonation. In Farinacci, A. (Ed.) - Proc. 2nd Int. Conf. Planktonic Microfossils Roma, 2: 739-785, Edizioni Tecnoscienza, Roma.

Martini E. & Worsley T. (1971) - Tertiary calcareous nannoplankton from the western equatorial Pacific. *In. Rep. Deep Sea Drilling Project*, 7: 1471-1507, Washington.

Miller K.G., Wright, J.D. & Fairbanks R.G. (1991) - Unlocking the Ice House: Oligocene-Miocene oxygen isotopes, eustasy, and margin erosion. *J. Geophys. Res.,* 96: 6829-6848, Washington.

Okada H. & Bukry D. (1980) - Supplementary modification and introduction of code numbers to the low-latitude coccolith biostratigraphic zonation. *Mar. Micropaleont.*, 5: 321-325, Amsterdam.

Olafsson G. (1989) - Quantitative calcareous nannofossil biostratigraphy of upper Oligocene to middle Miocene sediment from ODP Hole 667A and middle Miocene sediment from DSDP Site 574. *Proc. ODP, Sci. Results,* 108: College Station, TX (Ocean Drilling Program), pp. 9-22, College Station.

Olafsson G. & Villa G. (1992) - Reliability of sphenoliths as zonal markers in Oligocene sediments from the Atlantic and Indian Oceans. *Mem. Sci. Geol*, 43: 261-275, Padova.

Perch-Nielsen K. (1985) - Cenozoic calcareous nannofossils. In: Bolli, H.M., Saunders, J.B. & Perch-Nielsen, K. (Eds.) - Plankton Stratigraphy: 427-554, Cambridge Univ. Press, Cambridge.

Premoli Silva I. & Jenkins D.G. (1993) - Decision on the Eocene-Oligocene boundary stratotype. *Episodes,* 16: 379-381, Beijing.

Pälike H., Norris R.D., Herrle J.O., Wilson P.A., Coxall H.K., Lear C.H., Shackleton N.J., Tripati A.K. & Wade B.S. (2006) - The heartbeat of the Oligocene climate system. *Science,* 314: 1894-1898, Washington.

Raffi I., Backman J., Fornaciari E., Pälike H., Rio D., Lourens L.J. & Hilgen F.J. (2006) - A review of calcareous nannofossil astrobiochronology encompassing the past 25 Million years, *Quat. Sci. Rev.,* 25: 3113-3137, London.

Roth P.H., Franz H.E. and Wise S.W. Jr. (1971) - Morphological study of the selected members of the genus *Sphenolithus* Delfandre (Incertae sedis, Tertiary). In: Farinacci, A. (Ed.) - Proceedings of the II Planktonic Conference Roma 1970, 2: 1099-1119, Edizioni Tecnoscienza, Roma.

Shackleton N.J., Crowhurst S.J., Weedon G. & Laskar L. (1999) - Astronomical calibration of Oligocene-Miocene time. *Philos. Trans. R. Soc. Lond.*, 357: 1909-1927, London.

Shackleton, N.J., Hall, M.A., Raffi, I., Tauxe, L. & Zachos J. (2000) - Astronomical calibration for the Oligocene-Miocene boundary. *Geology*, 28: 447-450, Boulder.

Wade B.S. & Pälike H. (2004) - Oligocene climate dynamics. *Paleoceanography,* 19, Washington. PA4019. doi:10.1029/2004PA001042.

Wei W. & Wise S.W. Jr. (1989) - Paleogene calcareous nannofossil magnetobiochronology: results from South Atlantic DSDP Site 516. *Mar. Micropaleont.,* 14: 119-152, Amsterdam.

Wilson P.A., Lyle M., and Firth J.V. (Eds.) (2006) - *Proc. ODP, Sci. Results*, 199: College Station, TX (Ocean Drilling Program), College Station. doi:10.2973/odp.-proc.sr.199.2006

Young J. (2008) - www.nannotax.org

Zachos J.C., Pagani M., Sloan L.C., Thomas E. & Billups K. (2001) - Trends, rhythms, and aberrations in global climate 65 Ma to present. *Science*, 292: 686-693, Washington.

Appendix:

Alphabetic list of taxa encountered in this study:

Coccolithus pelagicus (Wallich, 1877) Schiller (1930)

Cyclicargolithus floridanus, (Roth & Hay in Hay et al., 1967) Bukry (1971a)

Dictyococcites bisectus (Hay, Mohler & Wade, 1966) Bukry & Percival (1971)

Dictyococcites hesslandii (Haq 1966), Haq & Lohman (1976)

Dictyococcites scrippsae Bukry & Percival (1971)

Discoaster barbadiensis Tan (1927)

Discoaster deflandrei Bramlette & Riedel (1954)

Discoaster saipanensis Bramlette & Riedel (1954)

Ericsonia formosa (Kamptner, 1963), Haq (1971)

Reticulofenestra umbilica (Levin, 1965) Martini & Ritzkowski (1968)

Reticulofenestra hillae Bukry & Percival (1971)

Sphenolithus ciperoensis Bramlette & Wilconxon (1967)

Sphenolithus distentus Martini (1965) Bramlette & Wilconxon (1967)

Sphenolithus predistentus Bramlette & Wilconxon (1967)

Sphenolithus moriformis (Brönnimann & Stradner, 1960) Bramlette & Wilconxon (1967)

Triquetrorhabdulus carinatus (Martini 1965)

Triquetrorhabdulus aff. *carinatus*